

Two-Layer Contact Nonlinear Mechanical Analysis of Flexible Drilling Tool in the Wellbore

Min Luo¹, Tingting Xu^{1,*}, Jiajun Jiang², Xu Chi³, Jing Wang⁴ and Shihua Xue¹

Abstract: The lack of research on flexible drilling tool leads to limited application of ultra-short radius horizontal wells. The flexible drilling tool is different from the conventional drilling tool. The flexible drilling pipe involves a mutual transition between the structure and the mechanism during the deformation process. At the same time, the flexible drilling pipe and the eccentric guide tube, the guide tube and the wellbore generate random contact. In this paper, 3-D beam elements, universal joint elements, rigid beam elements and the beam-beam contact elements are combined to establish a two-layer contact nonlinear finite element model of the flexible drilling tool in the wellbore. The dynamic relaxation method is introduced for numerical solution. The feasibility of the model and the algorithm is verified by an example. The mechanical analysis of flexible drilling tool under the four hole inclinations in the oblique section is carried out. It is found that the flexible drilling pipe has a “folded line” deformation. The contact force between the flexible drilling pipe and the guide tube is randomly distributed. The contact force between the guide tube and the wellbore in the oblique section is greater than that in the vertical section. As the hole inclinations increase, the torque and axial force transmitted to the drill bit gradually decrease.

Keywords: Flexible drilling tool, beam element, universal joint, contact nonlinear, finite element.

1 Introduction

The ultra-short radius horizontal well is an effective technique for developing potential residual oil. The obvious difference from the conventional horizontal well is that the radius of curvature is particularly small, generally 1 m-4 m. Conventional drilling tools cannot meet this requirement and require special techniques and tools for drilling. In the existing ultra-short radius horizontal well technology, two types of high-pressure jet tools [Wade, Herman, Nees et al. (1992); Buset, Riiber and Eek (2001); Bruni, Biassotti and

¹ Mechanical Science and Engineering College, Northeast Petroleum University, Daqing, 163318, China.

² Toutai Oilfield, Daqing Oil Field Co., Daqing, 163000, China.

³ Natural Gas Branch, the Third Group of Oil and Gas Processing, Daqing Oil Field Co., Daqing, 163453, China.

⁴ Mathematics and Statistics College, Northeast Petroleum University, Daqing, 163318, China.

* Corresponding Author: Tingting Xu. Email: 15246067500@163.com.

Received: 25 November 2019; Accepted: 07 January 2020.

Salomone (2007); Balch, Ruan, Savage et al. (2016); Wang, Li, Huang et al. (2016)] and flexible drilling tool [Gourley (2000); Zhang, Sun, Li et al. (2017); Lv (2018)] are mainly used. In engineering, flexible drilling tool generally adopt a two-layer flexible structure. The inner layer is a flexible pipe with controllable universal joint connection, which has the function of bearing pressure and transmitting torque. The outer layer is a single-sided slotted guide tube that transmits axial force. The structure of the main components of the flexible drilling tool is shown in Fig. 1.

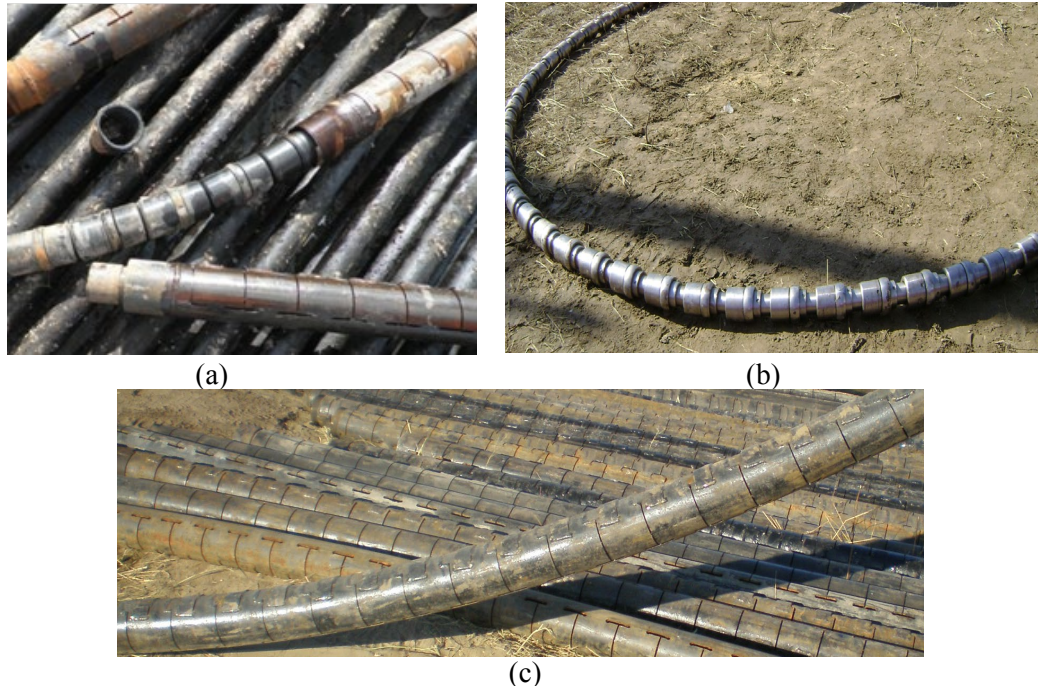


Figure 1: Structure of the main components of the flexible drilling tool: (a) Structure of the flexible drilling tool; (b) Structure of the flexible drilling pipe; (c) Structure of the guide tube

For flexible hinged pipes, scholars have carried out related mechanical analysis. Su et al. [Su and Zhao (1995); Zhao and Wang (1998)] regard the hinge joint as a plane hinge. A mechanical model of the hinged flexible drilling tool was created and the force condition at any hinge was derived through static analysis. Shuai et al. [Shuai and Liu (2001)] used the method of cohesive freedom to reduce the rotational freedom of the hinge point. A two-dimensional finite element model of the hinged drill assembly was established. Zhang et al. [Zhang and Di (2000); Di, Wang, Hu et al. (2012)] used the finite element iteration method to study the influence of the position of the hinge point on the dynamic characteristics of the bottom drilling tool. Liu et al. [Liu, Huang, Sun et al. (2016)] established a three-dimensional finite element model of flexible drilling pipe with different rotation angles. The ultimate tensile force and torque that the flexible drilling pipe can withstand was calculated.

For the beam-beam contact problem, Wriggers et al. [Wriggers and Zavarise (1997)] first proposed a frictionless contact model for studying the contact dynamics of a circular

section beam. Thereafter, Zavarise et al. [Zavarise and Wriggers (2000); Litewka and Wriggers (2002)] extended the model to the contact problems of circular section beams and rectangular section beams with Coulomb friction. Weyler et al. [Weyler, Oliver, Sain et al. (2012)] analyzed the advantages and disadvantages of the penalty function method and the Lagrangian method. It was finally established that the two methods were similar when dealing with beam and beam contact problems. Litewka proposed the Hermitian polynomial smoothing method and the multi-point contact method for beam-beam frictional contact [Litewka (2007, 2013)]. Neto et al. [Neto, Pimenta and Wriggers (2015)] proposed a self-contact model of beams using the pinball algorithm. Meier et al. [Meier, Popp and Wall (2016); Meier, Wall and Popp (2017)] developed a novel all-angle beam contact formula based on Kirchhoff beam theory. The point contact formula was applied in the large contact angles range while the line contact formula was applied in a small contact angle range. Liu et al. [Liu, Yue, Li et al. (1994); Liu, Luan and Zhang (2009)] described the random contact state between beam and beam by placing gap elements at the node locations to form a continuum between the beams. Pang et al. [Pang, Liu, Meng et al. (2009)] proposed a method for solving nonlinear finite element equation of beam-beam multi-directional contact by using the basic theory of cellular automata. Dong et al. [Dong, Zhang, Zhang et al. (2011)] applied movable two-way spring elements to describe the beam-beam contact state, and established a hybrid finite element simulation model describing the bending deformation law and contact pressure of the beams.

In summary, in the current study, the hinge is considered as a flat hinge, and the relative rotation angle limit is not considered in the hinge. The contact beams are all concentric section beams. While the hinge of the flexible drilling pipe can only be rotated at a fixed angle, and the flexible drilling pipe is accompanied by the mutual transition between the mechanism and the structure under the external load. The cross-section of the single-sided slotted guide tube is eccentric. The guide tube, the flexible drilling pipe and the wellbore form a three-body two-layer contact problem. How to reasonably describe the deformation state of flexible drilling tool, reveal its load transfer law, and establish the mechanical model and method of flexible drilling tool have certain difficulties. The relevant literature has not been reported.

For the flexible drilling tool in the wellbore, considering the transition between the flexible drilling pipe mechanism and the structure, the eccentricity of the guide tube section and the nonlinear characteristics of the two-layer contact, the finite element method is used to establish the finite element model of the flexible drilling tool in the wellbore. Aiming at the convergence difficulty in the calculation, the dynamic relaxation method is introduced to solve it. We validate the feasibility of the model and the algorithm by an example with analytical solutions. Through the mechanical analysis of the flexible drilling tool under the different hole inclinations for oblique drilling of ultra-short radius horizontal wells, we research the deformation state and load transfer law of the flexible drilling tool, and reveal the contact mechanics between the flexible drilling tool and the wellbore.

2 Finite element model and numerical solution method

2.1 Physical model

According to the drilling process of the flexible drilling tool in the oblique section, the mechanical analysis of flexible drilling tool under different hole inclinations is carried out. The structure of the flexible drilling tool is shown in Fig. 2. The flexible drilling tool consists of an upper triple connector, a flexible drilling pipe, a guide tube, a lower triple connector and a drill bit. The upper triple connector join the conventional drilling pipe, the flexible drilling pipe and the guide tube, while the lower triple connector join the drill bit, the flexible drilling pipe and the guide tube. During the oblique drilling process, the conventional drilling pipe transmits the axial force and torque to the upper triple connector, and the upper triple connector transmits the axial force to the guide tube and transmits the torque to the flexible drilling pipe, thereby the classification transmission of the load is realized. The lower triple connector transmits the axial force of the guide tube and the torque of the flexible drilling pipe to the drill bit, thereby the concentrated transmission of the loads is realized.

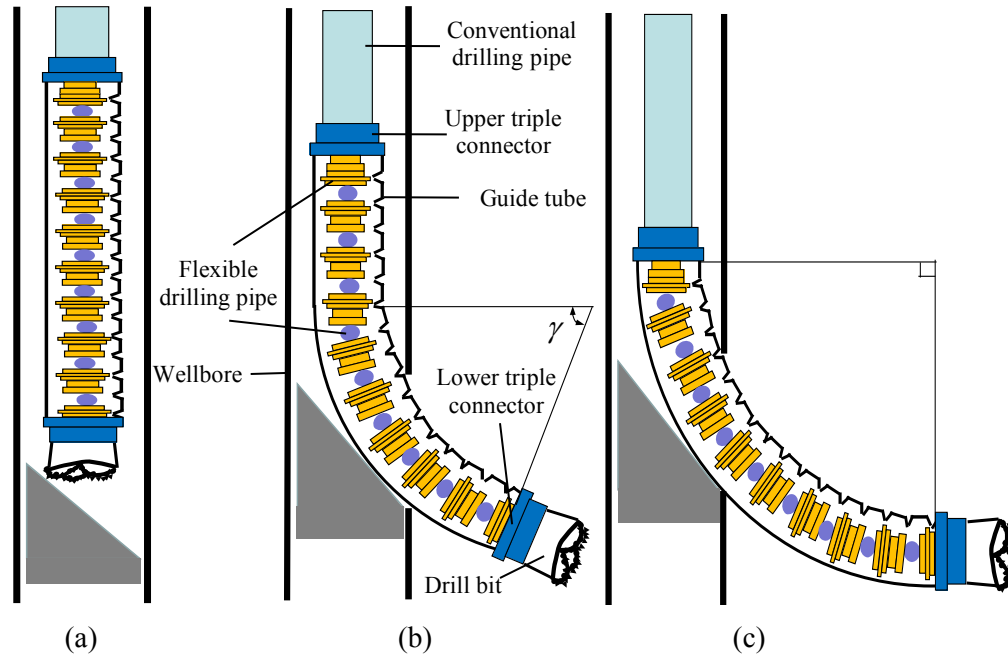


Figure 2: Structure of the flexible drilling tool under different hole inclinations: (a) $\gamma=0^\circ$; (b) $0^\circ < \gamma < 90^\circ$; (c) $\gamma=90^\circ$

The flexible drilling pipe and the guide tube are key components of flexible drilling tool, and their single-section structures are shown in Figs. 3(a) and 3(b), respectively. The units in the Fig. 3 are all mm.

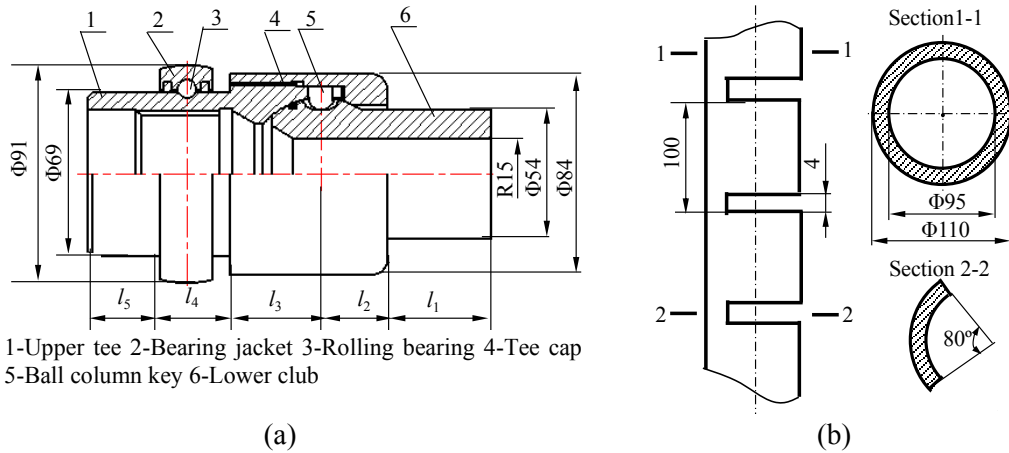


Figure 3: Structures of key components of flexible drilling tool: (a) Structure of single-section flexible drilling pipe; (b) Structure of single-section guide tube

2.2 Mechanical model

The following assumptions are made: (a) regardless of the threaded connection between the upper tee and the tee cap, they are integrated; (b) simplify the connection of the ball column keys and the sides to a controllable universal joint; (c) the influence of internal and external pressure difference is not considered; (d) the wellbore is treated as rigid bodies and fixed; (e) the flexible drilling pipe and the guide tube before deformation are located in the center of the wellbore; (f) the initial annular gap exists between the flexible drilling pipe, the guide tube and the wellbore; (g) the each component of the flexible drilling tool is simplified to a beam of the corresponding structural size.

Since this research focused on the contact state of the slender flexible drilling tool with the wellbore rather than the strength of the tool, to improve the calculation efficiency, the internal structure of the flexible drilling pipe is considered, and it is simplified into a cylindrical structure of the corresponding sectional size. The hinge is located at the junction of the sections S_2 and S_3 . The simplified structure is shown in Fig. 4.

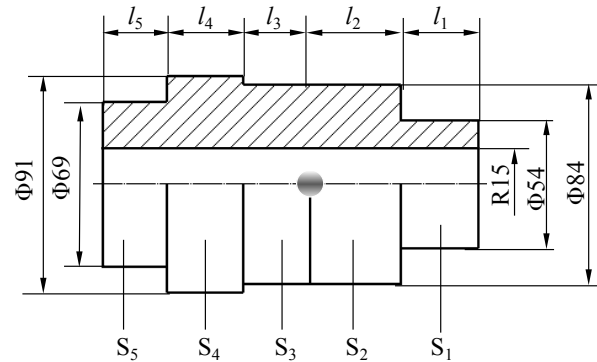


Figure 4: Simplified single-section flexible drilling pipe

The flexible drilling tool and the wellbore were selected as the research objects. According to the force characteristics of flexible drilling tool, the boundary condition is set as: The lateral line degrees of freedom of the drill bit are treated as contact boundaries with initial gaps, torsion and axial degrees of freedom are treated as fixed boundaries. The contact boundaries are used between the flexible drilling pipe and the guide tube, the guide tube and the wellbore, the triple connector and the wellbore, and the drill bit and the wellbore. The torque T and the axial force F at the upper triple connector are applied. Considering the weight q of flexible drilling tool, the mechanical model of the flexible drilling tool in the wellbore is shown in Fig. 5.

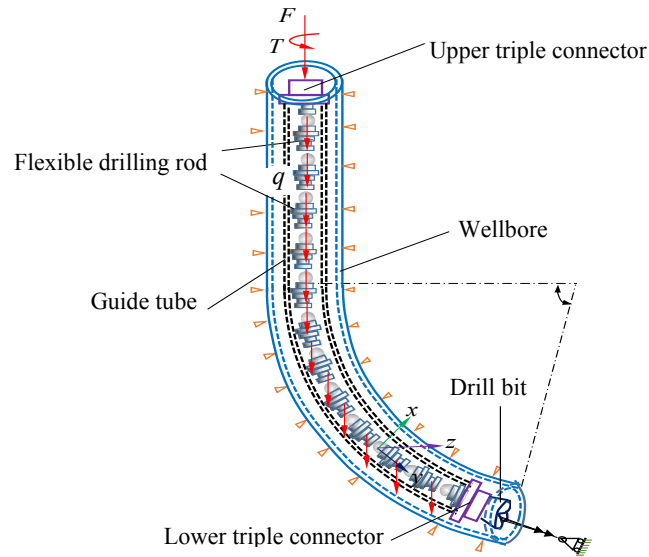


Figure 5: Mechanical model of flexible drilling tool in the wellbore

2.3 Finite element model

The flexible drilling pipe, guide tube, wellbore and other components of the flexible drilling tool are discretized into 3-D beam elements by finite element method. The 3-D beam elements are BEAM188 beam elements by ANSYS Release 17.0.

2.3.1 Finite element model of flexible drilling pipe

Given that the controllable universal joint can rotate relative to each other in the two directions, it is defined by two nodes. Nodes I and J are coincident. Each node has three translational displacements and three rotational displacements. The coordinate representation of the universal joint element is shown in Fig. 6. Two nodes need to define a local Cartesian coordinate system to describe the motion constraints. The y -axis is the direction of the drive shaft.

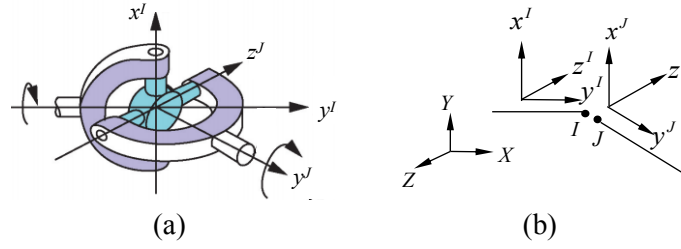


Figure 6: Coordinate representation of universal joint element: (a) Schematic diagram of universal joint structure; (b) Coordinate representation of the universal joint element

Since the displacement at the hinge is continuous, the displacement constraint of the universal joint element at any given time is expressed as

$$\mathbf{u}^I = \mathbf{u}^J \quad (1)$$

where \mathbf{u}^I and \mathbf{u}^J are the line displacement vectors of node I and node J , respectively.

Rotation constraint is expressed as

$$\mathbf{e}_x^I \mathbf{e}_z^J = 0 \quad (2)$$

where \mathbf{e}_x^I and \mathbf{e}_z^J are the unit vectors along the corresponding direction of each local coordinate system, respectively.

In order to measure the amount of change in the relative position of the local coordinate system of node I and node J , the initial position coincidence of local coordinate system of node I and node J is taken as an example to illustrate, as shown in Fig. 7. Assume that the local coordinate system of node I is unchanged. If the local coordinate system of node J rotates around the x -axis direction and its rotation angle is φ , the rotation angle φ is in the y - z plane. If the local coordinate system of the node J rotates around the z -axis direction and its rotation angle is ψ , the rotation angle ψ is located in the x - y plane.

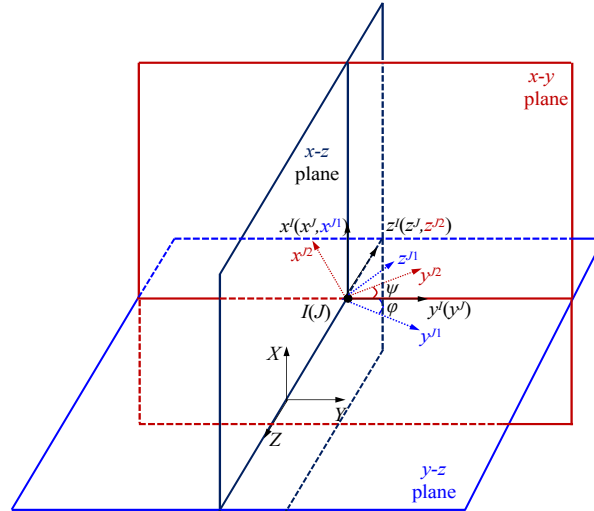


Figure 7: Relative position of node I and node J local coordinate system

Obviously, the first Carden angle (rotation angle around the x -axis direction) and the third Carden angle (rotation angle around the z -axis direction) of the relative position of the local coordinate system of the node I and the node J are respectively

$$\varphi = -\tan^{-1} \frac{\mathbf{e}_y^I \mathbf{e}_z^J}{\mathbf{e}_z^I \mathbf{e}_z^J}, \quad \psi = -\tan^{-1} \frac{\mathbf{e}_x^I \mathbf{e}_y^J}{\mathbf{e}_x^I \mathbf{e}_x^J} \quad (3)$$

The relative rotation angles of the two local coordinate systems are $\Delta\varphi$ and $\Delta\psi$, which can be expressed as

$$\Delta\varphi = \varphi - \varphi_0, \quad \Delta\psi = \psi - \psi_0 \quad (4)$$

where φ_0 and ψ_0 are the initial first and third Carden angles of the relative positions of the local coordinate systems of node I and node J .

When φ and ψ reach the rotation limit, the motion constraint of the universal joint element is expressed as

$$\mathbf{u}^I = \mathbf{u}^J, \quad \boldsymbol{\theta}^I = \boldsymbol{\theta}^J \quad (5)$$

where $\boldsymbol{\theta}^I$ and $\boldsymbol{\theta}^J$ are the angular displacement vectors of node I and node J , respectively.

It can be seen from the above analysis that the universal joint element has no shape function because the node positions are coincident. Its function is achieved only by given motion constraints. Combining the universal joint elements with the 3-D beam elements, the equilibrium equation of the flexible drilling pipe can be obtained.

According to the radius of curvature of the wellbore and the structure parameters of the flexible drilling pipe, the bending angle (initial first and third Carden angles) of the universal joint when the flexible drilling pipe is bent through the wellbore can be determined. The bending angle of the universal joint is defined by the local coordinate system. The plane where the axis of the wellbore is located is the XY plane, then the initial first Carden angle of each universal joint is zero, and the local coordinate system of the flexible drilling pipe universal joint is determined as shown in Fig. 8.

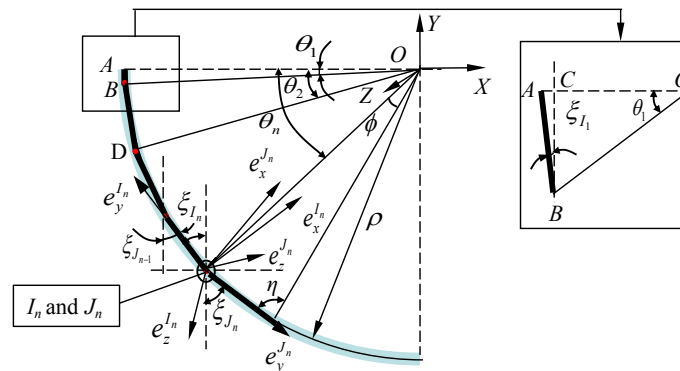


Figure 8: Local coordinate system at the universal joint

Suppose that the n th hinge consists of node I_n and node J_n , and the two nodes are coincident. $e_x^{I_n}, e_y^{I_n}, e_z^{I_n}, e_x^{J_n}, e_y^{J_n}$ and $e_z^{J_n}$ represent the local coordinate system of node I_n and node J_n , respectively. e_y is the direction of the drive shaft, e_x and e_y are perpendicular to each other in the XY plane, and e_z is perpendicular to the XY plane. ξ_{I_n} and ξ_{J_n} respectively represent the angle between the y direction of the node I_n and node J_n and the Y -axis direction of the global coordinate system, that is, the initial third Carden angle of the node I_n and node J_n . θ is the angle between the line connecting the universal joint and the center of curvature and the horizontal line.

The length of the single-section flexible drilling pipe is a , and the following relationship is satisfied.

$$a = l_1 + l_2 + l_3 + l_4 + l_5 \quad (6)$$

The length of the single-section flexible drilling pipe is small relative to the radius of curvature. It can be considered that the arc length corresponding to the single-section flexible drilling pipe is equal to the chord length a . According to the geometric relationship:

When $n=1$, in the $\triangle ABC$:

$$\cos \xi_{I_1} = \frac{BC}{AB} = \frac{\rho \sin \theta_1}{(l_1 + l_2)} \quad (7)$$

where $\theta_1 = (l_1 + l_2) / \rho$.

When $n > 1$

$$\begin{cases} \xi_{J_n} = \frac{\pi}{2} - (\eta - \theta_n) \\ \xi_{I_n} = \xi_{J_{n-1}} \end{cases} \quad (8)$$

where $\eta = \frac{\pi}{2} - \frac{\phi}{2} = \frac{\pi}{2} - \frac{a}{2\rho}$, $\theta_n = [l_1 + l_2 + (n-1)a] / \rho$.

The initial third Carden angle of each universal joint can be determined according to Eqs. (7) and (8), and the local coordinate system at the universal joint is also determined.

2.3.2 Finite element model of guide tube

The guide tube is discretized as 3-D beam elements. Based on the structural feature of the single-sided slotted guide tube, the complete circular section 1-1 and the eccentric section 2-2 are defined accordingly. The model of the guide tube is built as shown in Fig. 9. Taking the beam elements e_i and e_{i+1} as an example, the cross section of the e_i element is 1-1, and the cross section of the e_{i+1} element is 2-2. The inner and outer diameters of the two sections are equal. Element e_i consists of node i and node $i+1$. The element e_{i+1} consists of node $i+2$ and node $i+3$. At the intersection of the two beam element sections,

the nodes at the junction are not shared due to the different centroid positions, that is, the positions of node $i+1$ and node $i+2$ are different. The connection element e_j is introduced to meet displacement and load coordination at the junction. Obviously, the connection element consists of nodes $i+1$ and $i+2$, and the element has 12 degrees of freedom. Therefore, the connection element adopts the rigid beam element to achieve tension transfer, compression, bending, torsion and other forces [Laulusa, Bauchau, Choi et al. (2006)]. The rigid beam elements are MPC184 rigid beam elements by ANSYS Release 17.0. The guide tube is composed of a plurality of substructures of the same structure. The connection is established between the substructures through the connection element e_{j+1} . Combining the rigid beam elements with the 3-D beam elements, the equilibrium equation of the guide tube can be obtained.

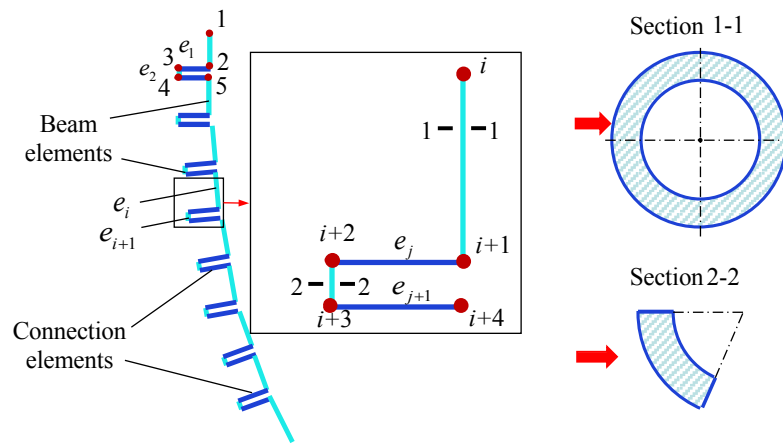


Figure 9: Analysis model of guide tube

2.3.3 Beam-to-beam contact

To analyze the contact problem of the flexible drilling pipe, the guide tube and wellbore, CONTA176 contact elements and TARGE170 target elements are created. The contact elements and the target elements are attached to the outer surface of the flexible drilling pipe and the inner surface of the guide tube, the outer surface of guide tube and the inner surface of the wellbore. The contact elements and the adherent 3-D beam elements satisfy the deformation coordination condition.

When contact occurs, the contact surface experiences normal contact pressure. Whether contact occurs between circular section beams can be defined by introducing a gap function to define the contact state of the two objects. When the gap function is less than zero, it reflects the existence of contact. The contact model of the beam in the beam is shown in Fig. 10.

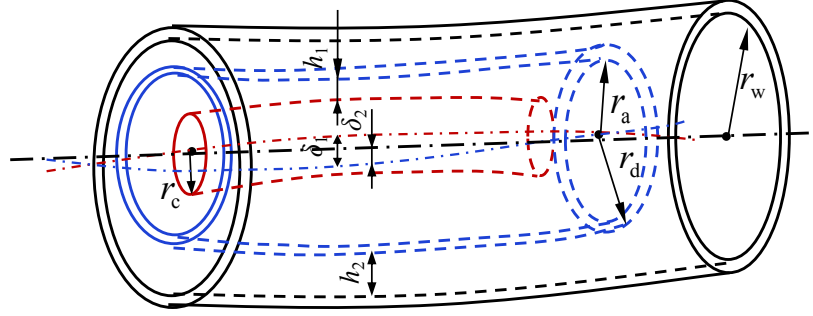


Figure 10: Contact model of beam in beam

Let the gap function between the flexible drilling pipe and the guide tube be h_1 . The gap function between the guide tube and the wellbore is h_2 . The gap function can be determined by the geometric relationship as:

$$\begin{cases} h_1 = r_a - r_c - \delta_1 \\ h_2 = r_w - r_d - \delta_2 \end{cases} \quad (9)$$

where r_w is the inner diameter of the wellbore; r_c is the outer diameter of the flexible drilling pipe; δ_1 and δ_2 are the minimum distance between the center line of the flexible drilling pipe and the center line of guide tube, the center line of the guide tube and center line of the wellbore, respectively.

The contact pairs satisfy the deformation coordination at the contact boundary. Based on the contact gap of the contact surface along the normal direction, the augmented Lagrangian algorithm is used to calculate the normal contact force.

2.3.4 Finite element model of flexible drilling tool in the wellbore

The elastic modulus, Poisson's ratio and density of the flexible drilling tool are 210 GPa, 0.3, and 7850 kg/m³, respectively. The length of the S₁-S₅ sections of the single-section flexible drilling pipe are 33 mm, 28 mm, 38 mm, 32 mm and 27 mm, respectively. The position of the hinge is between Section S₂ and Section S₃. The inner diameter of triple connector is 30 mm, the outer diameter is 110 mm, the length is $l_s=80$ mm. The inner diameter of the drill bit is 30 mm, the outer diameter is 118 mm, the length is $l_z=76$ mm. The inner diameter of the wellbore is 124 mm, and the outer diameter is 140 mm. The radius of curvature of the oblique section of the ultra-short radius horizontal well is $\rho=3.2$ m. Thus, the total length of the flexible drilling tool is given as $l=\rho\pi/2+2l_s+l_z$. The torque T is 2 kN·m. The axial force F is 40 kN.

Since the single-section flexible drilling pipe has five different sections, the single-section flexible drilling pipe is divided into five beam elements and one universal joint element. The single-section guide tube has two different sections, and one section is eccentric. The single-section guide tube is discretized into two beam elements and two rigid beam elements, and the wellbore is discretized into beam elements. The finite element model of the flexible drilling tool in the wellbore is shown in Fig. 11.

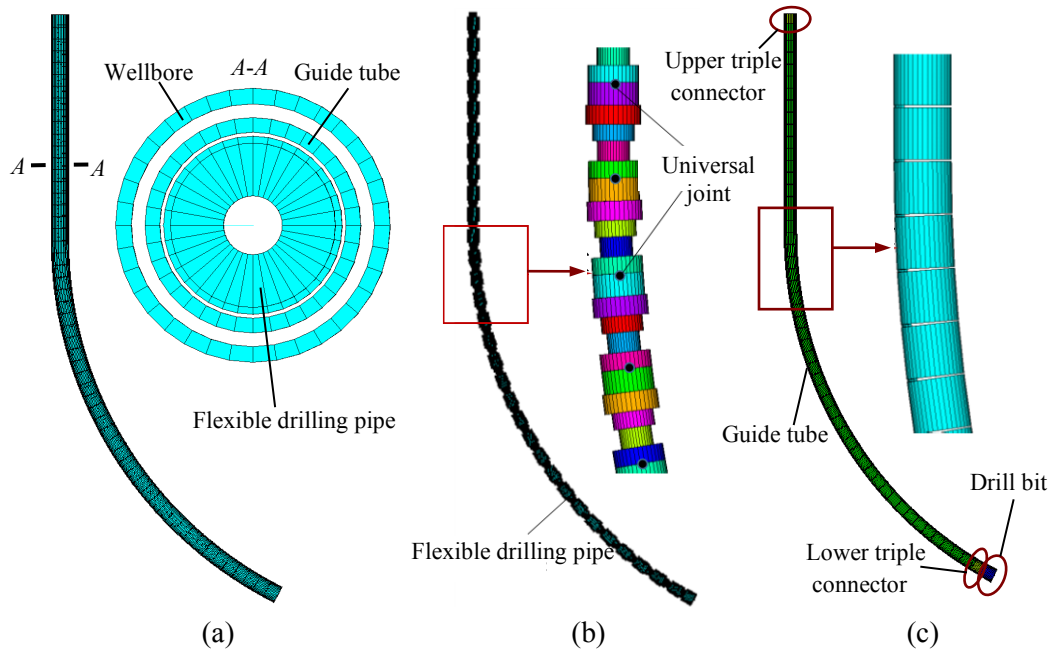


Figure 11: The finite element model of the flexible drilling tool in the wellbore: (a) Overall finite element model; (b) Finite element model of the flexible drilling pipe; (c) Finite element model of the guide tube

2.3.5 Dynamic relaxation method

The above finite element model is difficult to solve by ANSYS software. Specifically in the following aspects: (a) the strong nonlinear mechanical behavior such as contact and separation between the flexible drilling tool and the wellbore cause a sudden change in the contact state in the calculation process. This physical phenomena is easy to cause abnormal termination of calculation process and have difficulty in convergence; (b) the randomness of the universal joint movement and the unstable connection state, the beam is displaced by rigid body, which makes convergence difficult. To solve the convergent difficulty of flexible drilling tool in wellbore, we adopted a dynamic relaxation method for the nonlinear static contact analysis in ANSYS software. In this method, the dynamical method is used and larger damping is chosen [Zhang, Jiang, Huang et al. (2018)]. Calculation is stopped until the dynamic response of flexible drilling tool become stable. In other words, the flexible drilling tool in the wellbore static contact problem is solved by dynamical method.

3 Model verification

3.1 Model establishment

To verify the correctness of the controllable universal joint model, the two-layer contact analysis model and the algorithm, a planar model shown in Fig. 12 is established. There is a controllable hinge connection in the middle of the inner beam. The length of the beam is $2l$. The degree of rotation limit of the controllable hinge is β . The diameter of the

inner beam is d . The annulus gap between the inner beam and middle beam is Δ_1 . The annulus gap between the middle beam and the outer beam is Δ_2 . The thickness of the middle beam is t . The moments of inertia of the inner and middle beams are I_1 and I_2 , respectively. The elastic modulus of the inner beam and middle beam are both E . The left end of the inner beam is fully fixed, and the right end is a movable simply support. The left end of the middle beam is simply support and the right end is a movable simply support. The concentrated load F is applied at the hinge point of the inner beam.

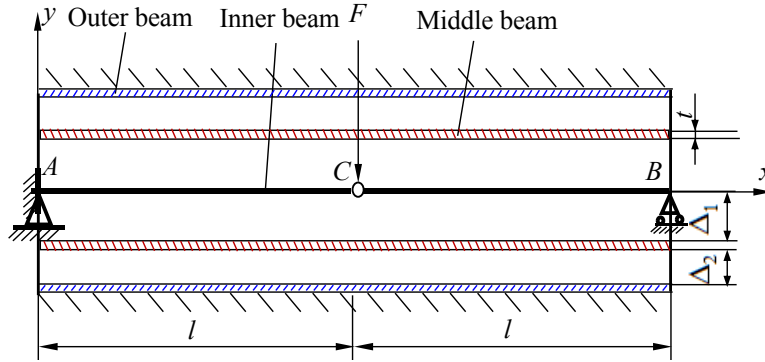


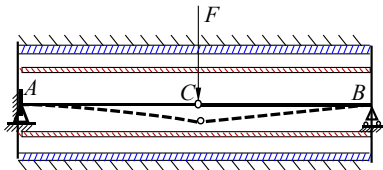
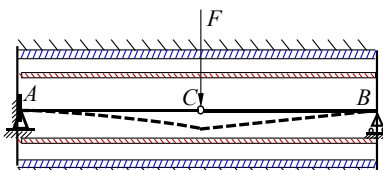
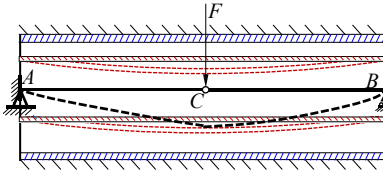
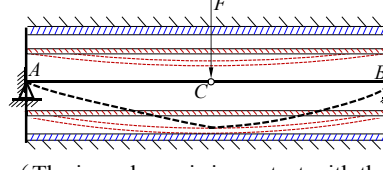
Figure 12: Beam-beam two-layer contact plane model

3.2 Theoretical analysis

Assume that the hinge of inner beam reaches the rotation limit degree and then comes into contact with the middle beam. According to the value of F , the contact state of the three beams can be divided into the following four cases as shown in Tab. 1. The dotted line is the bending deformation of the beam under concentrated load. Firstly, the inner beam is the research object. The critical concentration force is F_r when the hinge just reaches the degree of rotation limit. The deflection of the hinge point under the action of F_r is δ_r . To make the hinge of inner beam reach the rotation limit degree and then contact with the middle beam, the relationship $\Delta_1 > |\delta_r|$ should be satisfied. When the values of F are different, the contact states of the three beams are different. When the C point of the inner beam is just in contact with the middle beam, the critical force $F=F_1$. At this time, the deflection of the C point of the inner beam is $-\Delta_1$. When the middle beam is just in contact with the outer beam, the critical force $F=F_2$. At this time, the deflection of the C point of the inner beam is $-(\Delta_1 + \Delta_2)$, and the deflection of the middle beam corresponding to point C is $-\Delta_2$. The contact force between the inner beam and the middle beam is F_C . The contact force between the middle beam and the outer beam is F'_C . The bending moment at point C is M_C and the deflection is δ_C . According to the superposition principle, equilibrium equation and deformation coordination condition, deflection and bending moment of the hinge, contact forces between the beams under different values of F can be obtained. It should be pointed out that when $F > F_2$, the contact between the middle beam and the outer beam is actually a linear. For the

convenience of calculation, F is slightly larger than F_2 . It is assumed that a point contact is established between the middle and the outer beam, and the contact boundary is still processed as concentrated force. The expressions of the parameters are summarized in Tab. 1.

Table 1: Deformation conditions of beams under the action of different concentrated loads and the expressions of the parameters

F	Sketch of the beam	Parameters	Expressions
① $F \leq F_r$	 <p>(The inner beam does not reach the limit of rotation.)</p>	δ_C M_C F_C F'_C	$-\frac{Fl^3}{3EI_1}$ 0 0 0
② $F_r < F \leq F_1$	 <p>(The inner beam reaches the limit of rotation and does not come into contact with the middle beam.)</p>	δ_C M_C F_C F'_C	$-\frac{7Fl^3}{96EI_1} - \frac{5}{16}\beta l$ $\frac{5}{16}Fl - \frac{3EI_1\beta}{8l}$ 0 0
③ $F_1 < F \leq F_2$	 <p>(The inner beam is in contact with the middle beam, and the middle beam is not in contact with the outer beam.)</p>	δ_C M_C F_C F'_C	$-\frac{1}{16I_1 + 7I_2} \left(\frac{7Fl^3}{6E} + 5I_1\beta l - 7I_1\Delta_1 \right) - \frac{2}{5}\beta l$ $\frac{5I_1 l}{16I_1 + 7I_2} \left[F - \frac{6E\beta}{5l^2} (I_1 + 2I_2) + \frac{6EI_2\Delta_1}{l^3} \right]$ $\frac{I_2}{16I_1 + 7I_2} \left[7F + \frac{30EI_1\beta}{l^2} - \frac{96EI_1\Delta_1}{l^3} \right]$ 0
④ $F > F_2$	 <p>(The inner beam is in contact with the middle beam, and the middle beam is in contact with the outer beam.)</p>	δ_C M_C F_C F'_C	$-(\Delta_1 + \Delta_2)$ $\frac{EI_1}{7l^2} [30(\Delta_1 + \Delta_2) - 12\beta l]$ $F + \frac{EI_1}{7l^3} [30\beta l - 96(\Delta_1 + \Delta_2)]$ $F + \frac{EI_1}{7l^3} [30\beta l - 96(\Delta_1 + \Delta_2)] - \frac{6EI_2\Delta_2}{l^3}$

Given that: $E = 2.1 \times 10^{11}$ Pa, $d = 20$ mm, $l = 1$ m, $\beta = 1^\circ$, $t = 3$ mm, $\Delta_1 = 8$ mm, and $\Delta_2 = 3$ mm. $F_r = 34.48$ N, $F_1 = 57.49$ N and $F_2 = 390.96$ N can be obtained respectively. F is taken

as 20 N, 45 N, 200 N and 400 N, respectively. According to Tab. 1, theoretical solutions of deflections and bending moments at the hinge and contact forces between the beams under different lateral loads are shown in Tab. 2.

Table 2: Theoretical solutions of various parameters under different lateral loads

F/N	δ_c/mm	$M_c/\text{N}\cdot\text{m}$	F_c/N	F'_c/N
20	-4.04	0.00	0.00	0.00
45	-7.44	3.27	0.00	0.00
200	-9.18	16.25	113.48	0.00
400	-11.00	28.39	274.62	8.89

3.3 Numeral analysis

The above-mentioned controllable universal joint model, two-layer contact model and dynamic relaxation method are used to perform numerical analysis on the plane model. The boundary conditions of the plane model are shown in Tab. 3. It should be noted that the first Carden angle at the hinge of the inner beam is limited.

Table 3: The boundary conditions of the plane model

Category	Constrained position	UX	UY	UZ	ROTX	ROTY	ROTZ
Inner beam	<i>A</i>	√	√	√	√	√	√
	<i>B</i>		√	√	√	√	
Middle beam	<i>A</i>	√	√	√	√	√	
	<i>B</i>		√	√	√	√	
Outer beam	All nodes	√	√	√	√	√	√

The numerical solutions of deflections and bending moments at the hinge and contact forces between the beams under different lateral loads are shown in Tab. 4.

Table 4: Theoretical solutions of various parameters under different lateral loads

F/N	δ_c/mm	$M_c/\text{N}\cdot\text{m}$	F_c/N	F'_c/N
20	-4.04	0.00	0.00	0.00
45	-7.44	3.27	0.00	0.00
200	-9.29	16.30	113.30	0.00
400	-11.00	28.50	274.24	9.23

3.4 Error analysis

For the beam-to-beam two-layer contact plane model, the results of theoretical and numerical analysis of deflections and bending moments at the hinge and contact forces between the beams are shown in Tab. 5.

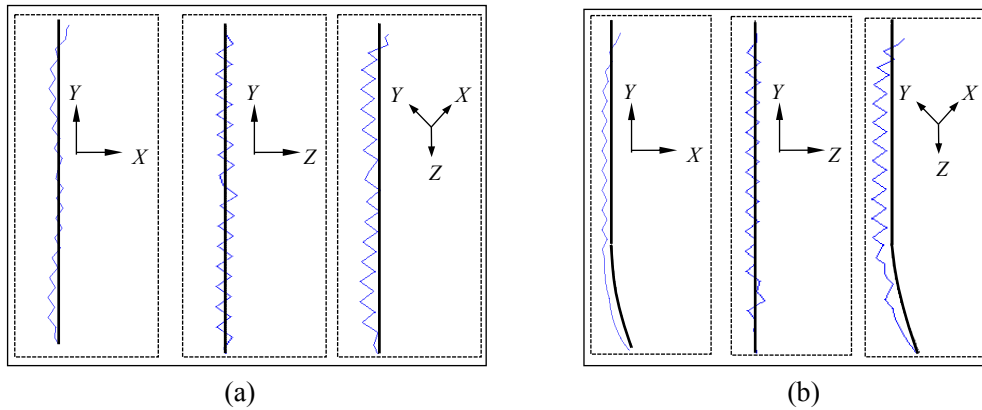
Table 5: Comparison of theoretical solutions and numerical solutions

F/N	Error/%			
	δ_c	M_c	F_c	F'_c
20	0.00	0.00	0.00	0.00
45	0.00	0.00	0.00	0.00
200	1.20	0.31	0.16	0.00
400	0.00	0.39	0.14	3.80

It can be seen from Tab. 5 that the maximum error of the theoretical solution and the numerical solution is only 3.8%, which verifies the feasibility of the model and the algorithm.

4 Result and discussion

Through mechanical analysis of flexible drilling tool in the wellbore with hole inclinations γ of 0° , 30° , 60° and 90° , we obtain the deformation form of the flexible drilling pipe in different coordinate planes as shown in Fig. 13. The third Cardan angle and the first Cardan angle of the flexible drilling pipe universal joint are as shown in Fig. 14. The contact force between the flexible drilling pipe and the guide tube is as shown in Fig. 15. The torque and axial force distribution of the flexible drilling pipe are shown in Figs. 16 and 17.



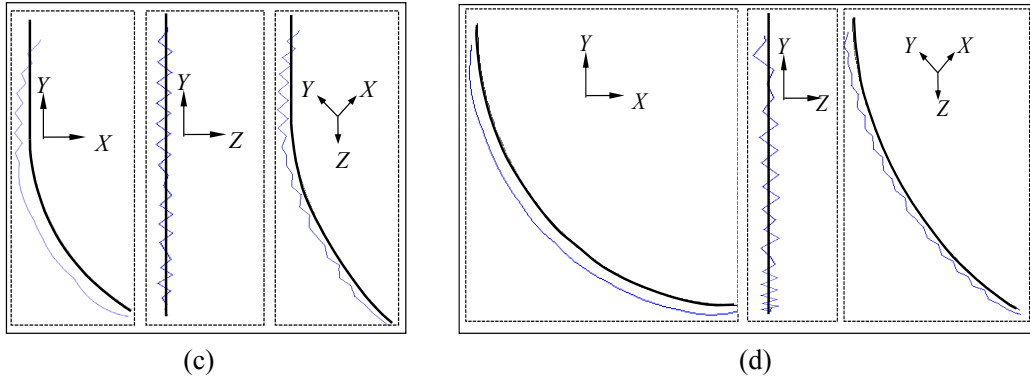
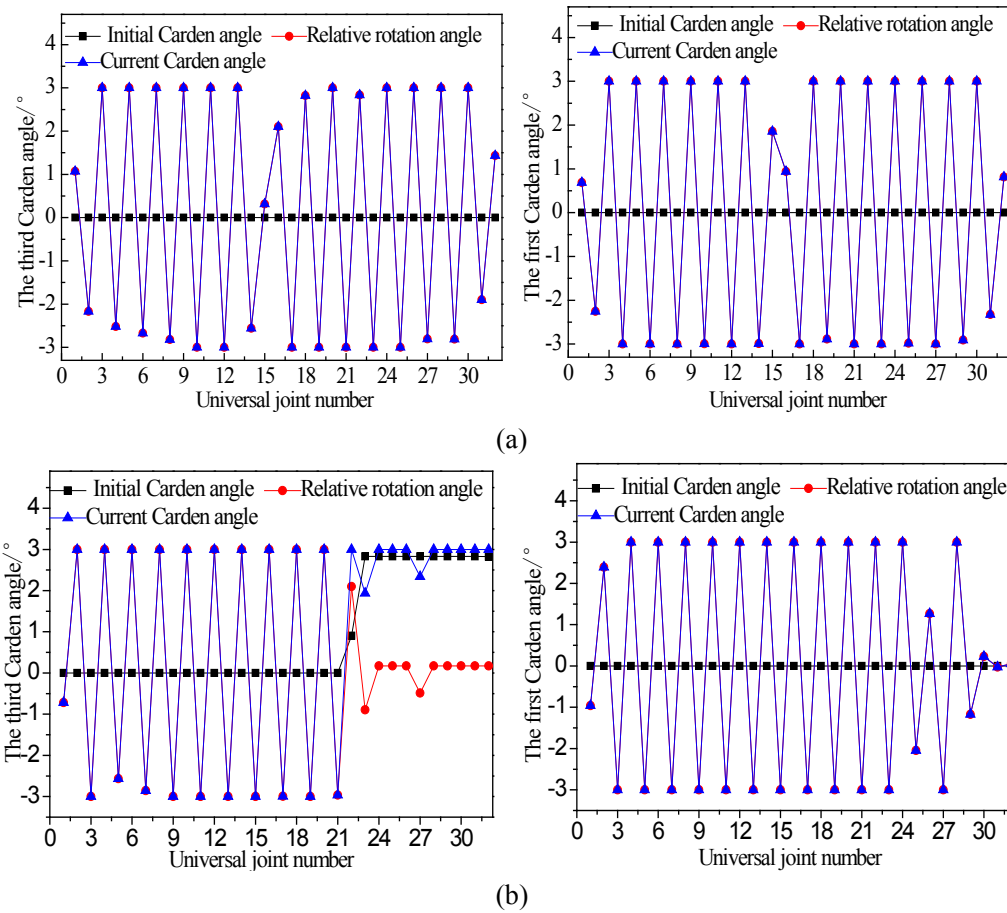


Figure 13: Deformation of flexible drilling pipe in different coordinate planes: (a) $\gamma=0^\circ$; (b) $\gamma=30^\circ$; (c) $\gamma=60^\circ$; (d) $\gamma=90^\circ$



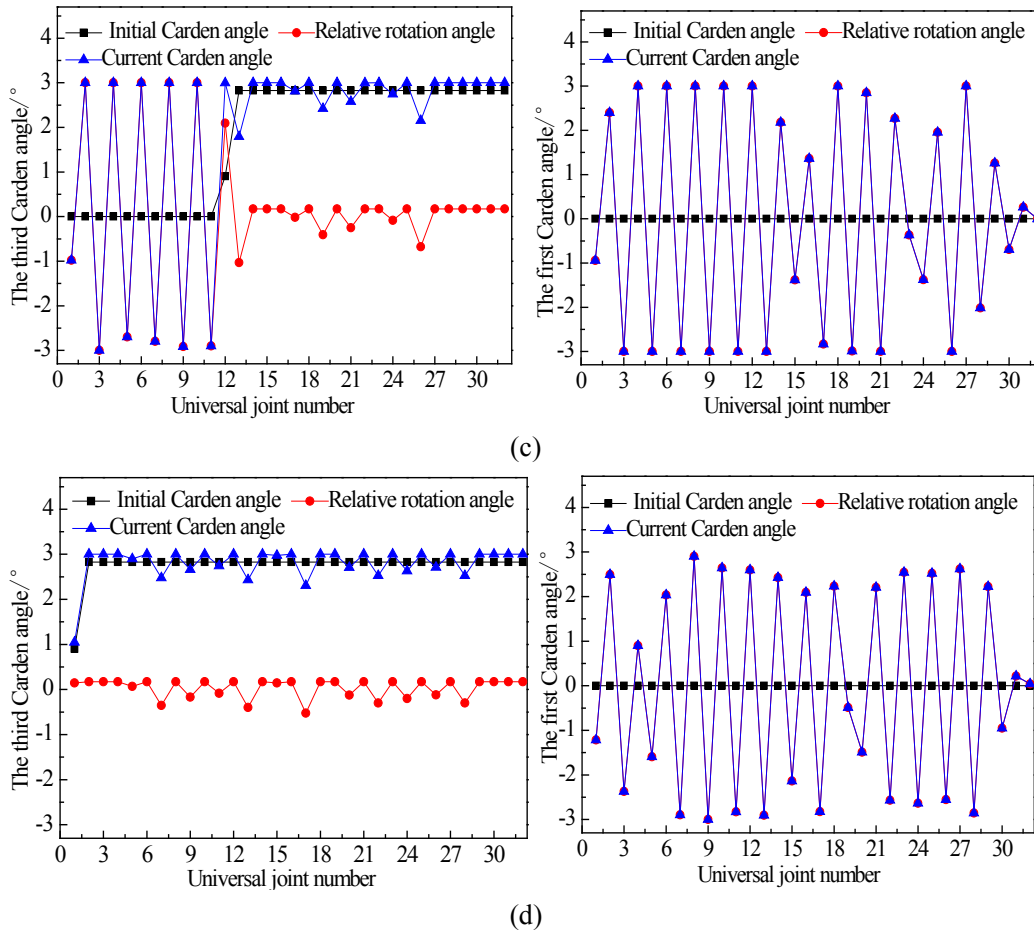


Figure 14: Carden angle of universal joint: (a) $\gamma=0^\circ$; (b) $\gamma=30^\circ$; (c) $\gamma=60^\circ$; (d) $\gamma=90^\circ$

It can be seen from Figs. 13 and 14 that the “folded line” deformation of the vertical section of the flexible drilling pipe in the XY plane is more obvious than that of the oblique section under the four hole inclinations, because the initial third Carden angle of the vertical section of the universal joint is zero, but the initial third Carden angle of the oblique section is not zero. Under the rotation limit of 3° , the relative rotation angle of the vertical flexible drilling pipe is larger than that of the oblique section, thus the deformation is more obvious. The “folded line” deformation of the vertical section and the oblique section of the flexible drilling pipe in the YZ plane are both obvious. This is because the initial first Carden angle of the vertical section and the oblique section are both zero and the relative rotation angles are both large. Since the initial first Carden angle of the universal joint is zero, the current first Carden angle is equal to the relative rotation angle. Most of the current Carden angles of the universal joint reach rotation limit. The top end of the flexible drilling pipe is inclined in the positive direction of the X -axis. This is because the slits of the guide tube are closed under the reaction of the axial force, and line displacements degree of freedom of the top nodes of the flexible drilling

pipe and the guide tube are coupled through the upper triple connector, and the line displacements in the three directions are equal. Thus, the top of the flexible drilling pipe would produce lateral bending along with the guide tube.

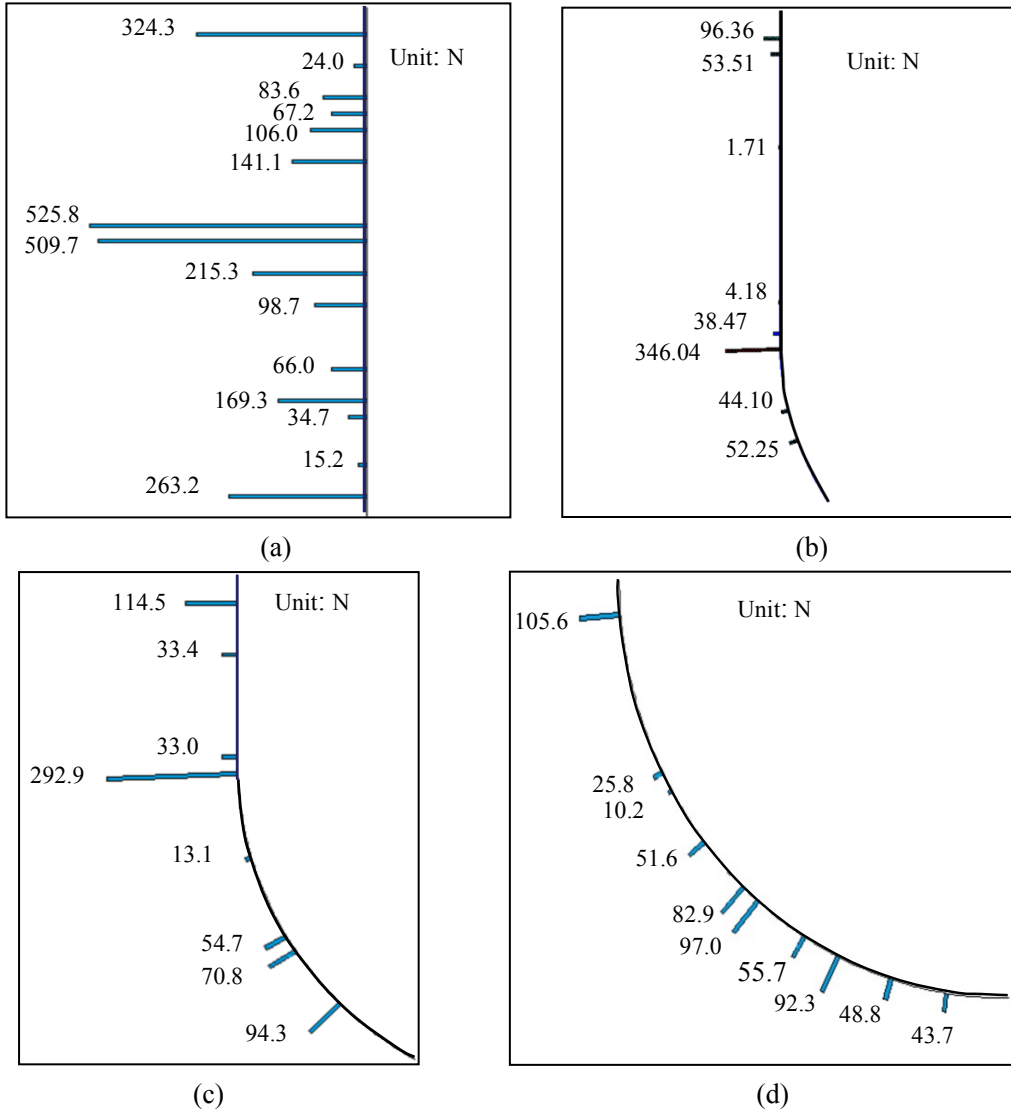


Figure 15: Distribution of contact between flexible drilling pipe and guide tube: (a) $\gamma=0^\circ$; (b) $\gamma=30^\circ$; (c) $\gamma=60^\circ$; (d) $\gamma=90^\circ$

It can be seen from Fig. 15 that the contact force between the flexible drilling pipe and the guide tube is randomly distributed, and only the maximum cross section of the flexible drilling pipe is in contact with the guide tube. The maximum contact force is in the vertical section. This is due to the fact that the guide tube slit closure of the vertical section causes its shortened distance to be greater than the oblique section. That is, the

shortened distance of flexible drilling pipe of the vertical section shortens is greater than the oblique section. The hinged connection results in a large radial displacement of the flexible drilling pipe. Therefore, when $\gamma=0^\circ$, the contact force between the flexible drilling pipe and the guide pipe is the largest, and the contact area is large.

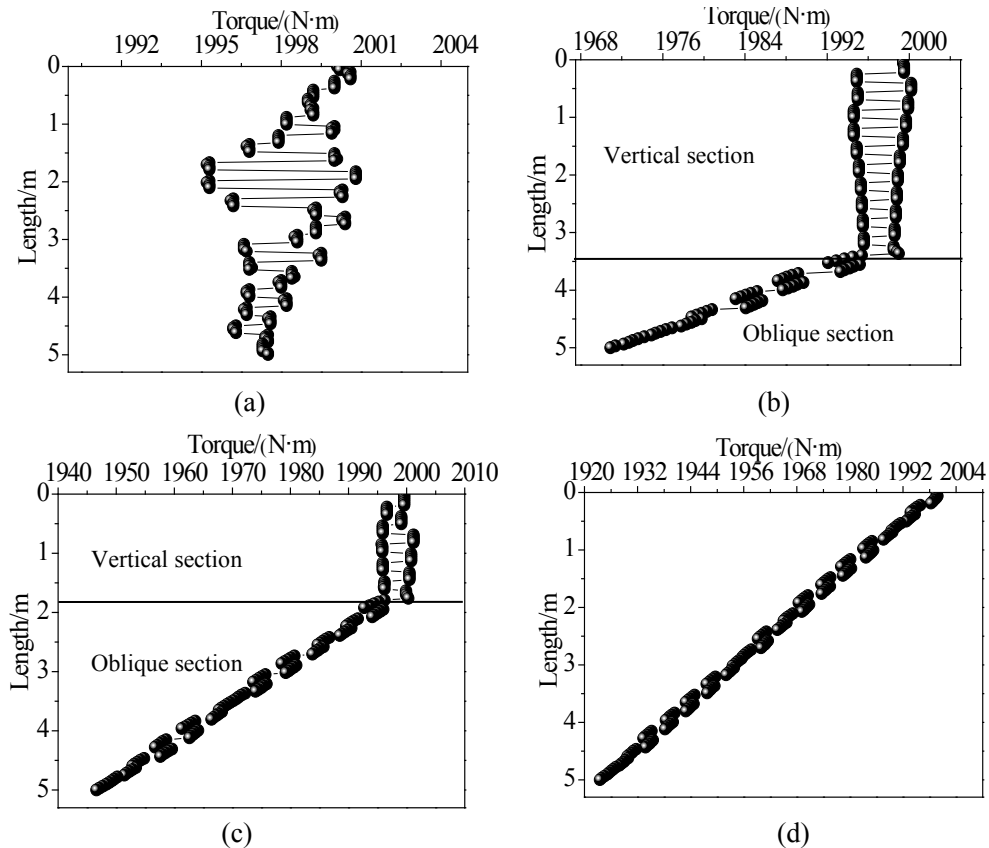


Figure 16: Torque distribution of flexible drilling pipe: (a) $\gamma=0^\circ$; (b) $\gamma=30^\circ$; (c) $\gamma=60^\circ$; (d) $\gamma=90^\circ$

Fig. 16 shows that the torque of the flexible drilling pipe in the vertical section fluctuates around 2000 N·m, and the change is small. The torque of the flexible drilling pipe in the oblique section gradually decreases. The torque loss of a flexible drilling pipe consists of two parts: one part is the frictional torque generated by the circumferential friction, which causes torque loss, which is unrecoverable. However, the torque loss caused by friction is small. The other part is that the universal joint drive shaft is not in a straight line, and there is a certain angle. The angle between the universal joint drive shafts at different positions increases the torque and some reduces the torque. The positive and negative values of the third Carden angles and the first Carden angles of the vertical section universal joint are equivalent, that is, the value of the flexible drilling pipe torque increase is substantially equal to the reduced value. Therefore, the torque loss of the vertical section of the flexible drilling pipe is small. The positive and negative values of

the first Cardan angles of the oblique section universal joint are equivalent. However, the third Cardan angles are positive, so the torque of the flexible drilling pipe is gradually reduced. When the hole inclinations are 0° , 30° , 60° and 90° , the torque values at the bottom end of the flexible drilling pipe are 1997 N·m, 1971 N·m, 1947 N·m and 1924 N·m, respectively. The torque loss rates are 0.2%, 1.5%, 2.7%, and 3.8%, respectively.

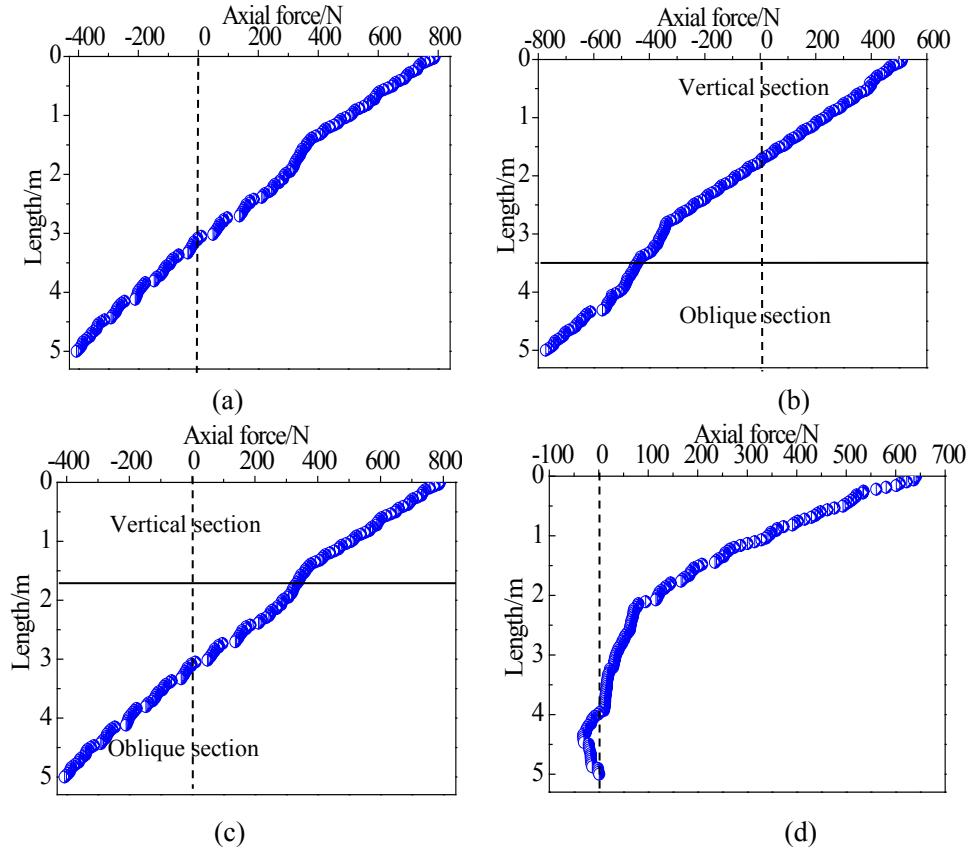


Figure 17: Axial force distribution of flexible drilling pipe: (a) $\gamma=0^\circ$; (b) $\gamma=30^\circ$; (c) $\gamma=60^\circ$; (d) $\gamma=90^\circ$

Fig. 17 shows that the axial force of the flexible drilling pipe under the four hole inclinations has a neutral point. This is because the shortened distance between the flexible drilling pipe and the guide tube are equal. When the guide tube slits are completely closed, the flexible drilling pipe have universal joints that don't reach the rotation limit. The flexible drilling pipe is also subjected to its own weight, so the top end of the guide tube supports the flexible drilling pipe, causing the upper part of the flexible drilling pipe to be pulled and the lower part to be pressed. As the hole inclinations of the well increases, the force from self-weight decomposition to axial direction of the flexible drilling pipe gradually decreases, and the pressed area gradually decreases.

The deformation form of the guide tube is as shown in Fig. 18. The contact force between the guide tube and the wellbore is as shown in Fig. 19. The axial force distribution law of the guide tube is as shown in Fig. 20.

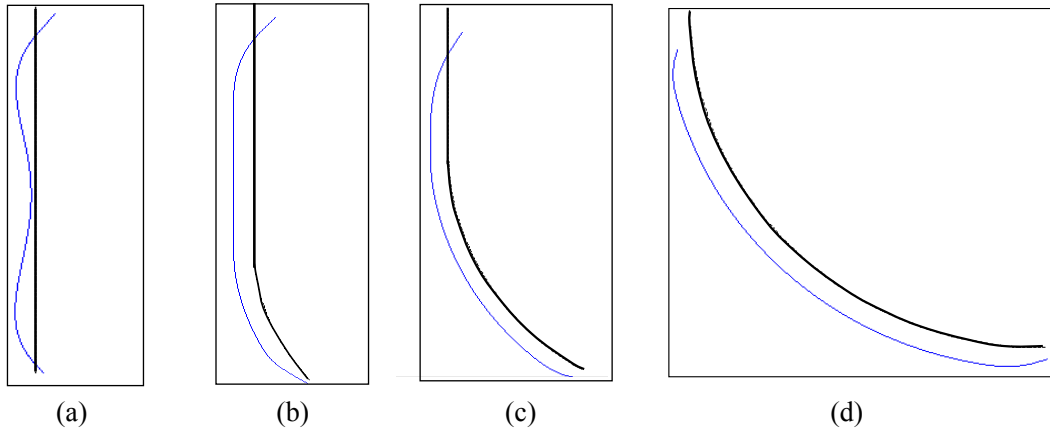


Figure 18: Deformation of guide tube: (a) $\gamma=0^\circ$; (b) $\gamma=30^\circ$; (c) $\gamma=60^\circ$; (d) $\gamma=90^\circ$

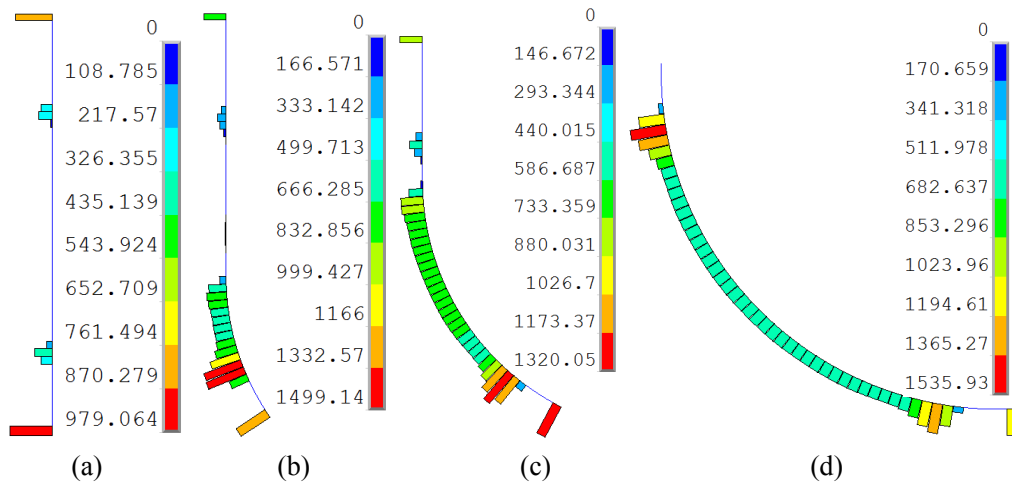


Figure 19: Contact force distribution between guide tube and wellbore: (a) $\gamma=0^\circ$; (b) $\gamma=30^\circ$; (c) $\gamma=60^\circ$; (d) $\gamma=90^\circ$

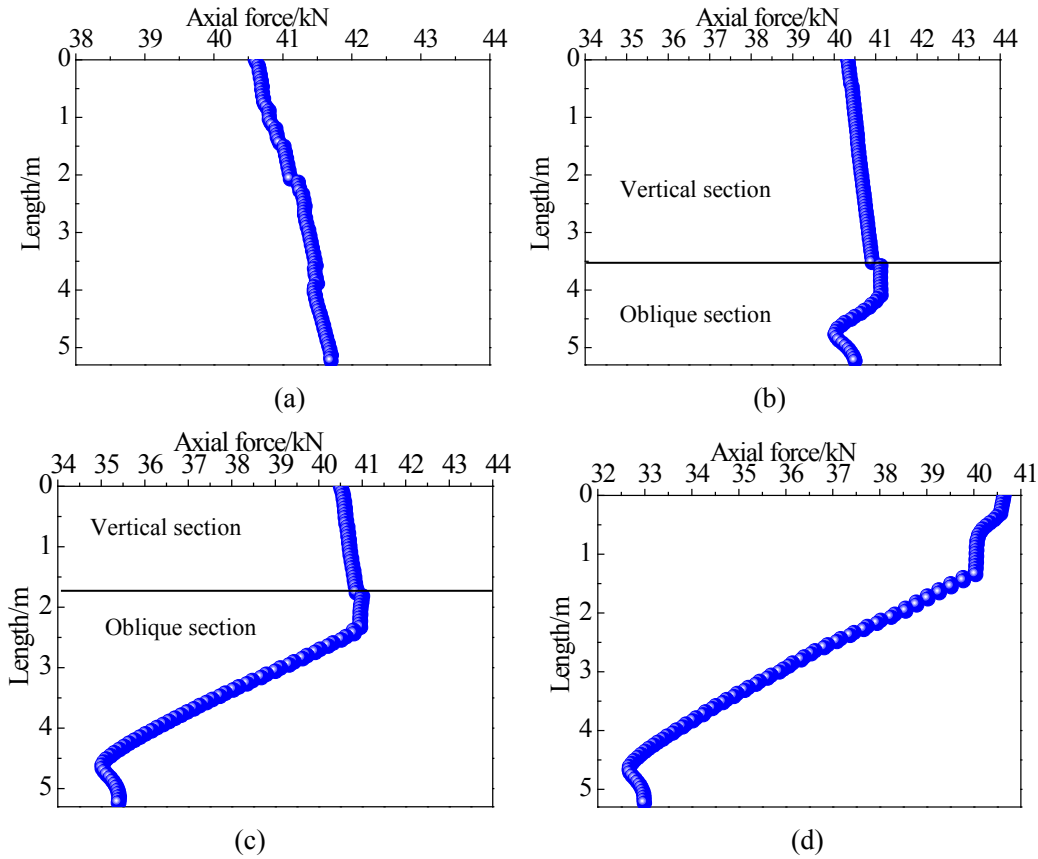


Figure 20: Axial force distribution of guide tube: (a) $\gamma=0^\circ$; (b) $\gamma=30^\circ$; (c) $\gamma=60^\circ$; (d) $\gamma=90^\circ$

It can be seen from Fig. 18 to Fig. 20 that the triple connector on the top end of the guide tube is inclined in the positive direction of the X axis. This is because the guide tube is laterally bent due to the axial force. When hole inclinations are 0° , 30° and 60° , the upper triple connector on the guide tube is in contact with the wellbore, and the guide tube near the upper triple connector is not in contact with the wellbore. When hole inclination is 90° , the radial displacement of the upper triple connector is smaller than the annular space between the guide tube and the wellbore, and the triple connector is not in contact with the wellbore. Due to the support of the drill bit, the guide tube near the drill bit do not come into contact with the wellbore. The contact area of the oblique section between the guide tube and the wellbore is larger than that of the vertical section. The axial force of the vertical section guide tube is gradually increased, and the axial force near the top end of the oblique section guide tube is firstly stabilized. As the length increases, the axial force gradually decreases, and then increases. The change of the axial force of the guide tube is determined by the contact force between the guide tube and the wellbore. If the axial force of the self-weight decomposition of the guide tube is greater than the axial cumulative frictional resistance, the axial force of the guide tube will increase, and vice versa. The axial force transmitted to the drill bit is the sum of the axial forces of the

bottom end of the guide tube and the flexible drilling pipe. When the hole inclinations are 0° , 30° , 60° and 90° , the axial forces transmitted to the drill bit are 42.11 kN, 41.28 kN, 35.80 kN and 32.99 kN, respectively.

5 Conclusions

(1) Based on the structural characteristics of the flexible drilling tool, considering the mechanism and structural transition of the flexible drilling pipe, the eccentricity of the guide tube section and the nonlinear characteristics of the two-layer contact, 3-D beam elements, universal joint elements, rigid beam elements and the beam-beam contact elements are combined to establish a two-layer contact nonlinear finite element model of the flexible drilling tool in the wellbore. In order to solve the problem of convergence in the calculation process of finite element model, the dynamic relaxation method is introduced for numerical solution.

(2) A two-layer contact plane model of inner beam with a controllable hinge and middle beam and outer beam is established. In the case where the inner beam is subjected to different lateral loads at the controllable hinge, based on the superposition principle, equilibrium equation and deformation coordination conditions, deflection and bending moment at the controllable hinge and the contact force between the beams are derived. Comparing the theoretical solution with the numerical solution, the maximum error is only 3.8%, which verifies the feasibility of the model and numerical calculation method of the flexible drilling tool in the wellbore.

(3) The deformation of the hinged flexible drilling pipe exhibited a “folded line” deformation with respect to the initial configuration. The contact force between the flexible drilling pipe and the guide tube is randomly distributed, and only the largest sections of the flexible drilling pipe are in contact with the guide tube. As the length increased, the torque of the flexible drilling pipe of the vertical section did not change much, and the torque of the flexible drilling pipe of the oblique section gradually decreased. The contact force between the guide tube and the wellbore of the vertical section is smaller than that of the oblique section. As the length increased, the axial force of guide tube of the vertical section gradually increased, and the axial force of guide tube of the oblique section gradually decreased. As the hole inclinations increases, the torque and axial force transmitted to the drill bit gradually decrease. When the hole inclination is 90° , loss rates of the torque and the axial force transmitted to the drill bit are 3.8% and 17.5%, respectively.

Acknowledgement: The authors gratefully acknowledge the financial support from the Natural Science Foundation of China (Grant numbers: 51674088).

Funding Statement: The work has been supported by National Natural Science Foundation of China (Grant No. 51674088). The author who received the grant is Luo, M. The URL to sponsor’s website: <http://www.nsf.gov.cn/>.

Conflicts of Interest: The authors declare that they have no conflicts of interest to report regarding the present study.

References

- Buset, P.; Riiber, M.; Eek, A.** (2001): Jet drilling tool: cost-effective lateral drilling technology for enhanced oil recovery. *SPE/ICOTA Coiled Tubing Roundtable*, Houston. Society of Petroleum Engineers.
- Bruni, M.; Biassotti, H.; Salomone, G.** (2007): Radial drilling in Argentina. *SPE 10th Latin American & Caribbean Petroleum Engineering Conference*, Buenos Aires. Society of Petroleum Engineers.
- Balch, R. S.; Ruan, T.; Savage, M.; Havard, J.** (2016): Field testing and validation of a mechanical alternative to radial jet drilling for improving recovery in mature oil wells. *SPE Western Regional Meeting*, Alaska. Society of Petroleum Engineers.
- Di, Q. F.; Wang, M. J.; Hu, Y. B.; Zhao, Y. D.; Zhu, W. P. et al.** (2012): Effect of flex sub's position on bottom hole assembly with rotary steering tool. *Journal of China University of Petroleum (Edition of Natural Science)*, vol. 36, no. 5, pp. 84-88.
- Dong, S. M.; Zhang, W. S.; Zhang, H.; Wang, C. F.** (2011): Research on the distribution contact pressure between sucker rod and tubing string of rod pumping system in directional wells. *Engineering Mechanics*, vol. 28, no. 10, pp. 179-184.
- Gourley, G.** (2000): Flexible drilling tool may aid in enhanced oil recovery. In *SPE Permian Basin Oil and Gas Recovery Conference*, Midland. Society of Petroleum Engineers.
- Laulusa, A.; Bauchau, O. A.; Choi, J. Y.; Tan, V. B. C.; Li, L.** (2006): Evaluation of some shear deformable shell elements. *International Journal of Solids and Structures*, vol. 43, no. 17, pp. 5033-5054.
- Litewka, P.** (2007): Hermite polynomial smoothing in beam-to-beam frictional contact. *Computational Mechanics*, vol. 40, no. 5, pp. 815-826.
- Litewka, P.** (2013): Enhanced multiple-point beam-to-beam frictionless contact finite element. *Computational Mechanics*, vol. 52, no. 6, pp. 1365-1380.
- Litewka, P.; Wriggers, P.** (2002): Contact between 3D beams with rectangular cross-sections. *International Journal for Numerical Methods in Engineering*, vol. 53, no. 9, pp. 2019-2041.
- Liu, H.; Huang, S. Z.; Sun, Q.; Ming, E.; Li, T. et al.** (2016): Application of ultra short radius lateral drilling technique in top thick reservoir exploitation after long term water flooding. *Abu Dhabi International Petroleum Exhibition & Conference*, Abu Dhabi. Society of Petroleum Engineers.
- Liu, J. B.; Yue, Q. B.; Li, Z. M.; Luo, M.** (2009): The analysis and application of double layer contact finite element about rod and tubing string well bore. *Mechanics in Engineering*, vol. 31, no. 2, pp. 35-39.
- Liu, J. B.; Luan, S. X.; Zhang, X. H.** (1994): Mechanics and deformation analysis for the fracturing string in a horizontal well using gap element method. *Acta Petrolei Sinica*, vol. 15, no. 1, pp. 135-140.
- Lv, M.** (2018): Ultra-short radius multi-branch horizontal well sidetracking technology based on flexible drilling tool and its application. *China Petroleum and Chemical Standard and Quality*, vol. 38, no. 20, pp. 156-157.

- Meier, C.; Popp, A.; Wall, W. A.** (2016): A finite element approach for the line-to-line contact interaction of thin beams with arbitrary orientation. *Computer Methods in Applied Mechanics & Engineering*, vol. 308, pp. 377-413.
- Meier, C.; Wall, W. A.; Popp, A.** (2017): A unified approach for beam-to-beam contact. *Computer Methods in Applied Mechanics & Engineering*, vol. 315, pp. 972-1010.
- Neto, A. G.; Pimenta, P. M.; Wriggers, P.** (2015): Self-contact modeling on beams experiencing loop formation. *Computational Mechanics*, vol. 55, no. 1, pp. 193-208.
- Pang, D. X.; Liu, Q. Y.; Meng, Q. H.; Wang, G. R.** (2009): Solving method for nonlinear contact problem of drill strings in 3D curved borehole. *Acta Petrolei Sinica*, vol. 30, no. 1, pp. 121-124.
- Shuai, J.; Liu, C.** (2001): Dynamic analysis of the hinged bottom hole assembly. *Oil Field Equipment*, vol. 30, no. 5, pp. 15-18.
- Su, Y. N.; Zhao, J. P.** (1995): Establishment and analysis of mechanical model of articulated downhole motor assembly for short radius horizontal well. *Oil Drilling & Production Technology*, vol. 17, no. 4, pp. 25-33.
- Wade, D.; Herman, D.; Nees, J. M.; Eric, D.** (1992): The ultrashort radius radial system applied to thermal recovery of heavy oil. *Proceedings of the Eighth Symposium on Enhanced Oil Recovery, California*. Society of Petroleum Engineers.
- Wang, B.; Li, G. S.; Huang, Z. W.; Li, J. B.; Zhng, D. B. et al.** (2016): Hydraulics calculations and field application of radial jet drilling. *SPE Drilling & Completion*, vol. 31, no. 1, pp. 71-81.
- Weyler, R.; Oliver, J.; Sain, T.; Cante, J. C.** (2012): On the contact domain method: a comparison of penalty and Lagrange multiplier implementations. *Computer Methods in Applied Mechanics & Engineering*, vol. 205, no. 1, pp. 68-82.
- Wriggers, P.; Zavarise, G.** (1997): On contact between three-dimensional beams undergoing large deflections. *Communications in Numerical Methods in Engineering*, vol. 13, no. 6, pp. 429-438.
- Zavarise, G.; Wriggers, P.** (2000). Contact with friction between beams in 3-D space. *International Journal for Numerical Methods in Engineering*, vol. 49, no. 8, pp. 977-1006.
- Zhao, J. P.; Wang, X. H.** (1998): Mechanical analysis of articulated drilling string for small-radius horizontal well. *Journal of Northeast Petroleum University*, vol. 22, no. 3, pp. 26-27.
- Zhang, S. L.; Sun, Q.; Li, T.; Ming, E. Y.; Huang, S. Z. et al.** (2017): The low cost ultra-short radius sidetracking technology in produced wells based on flexible drilling pipe. *China Petroleum Machinery*, vol. 45, no. 12, pp. 18-22.
- Zhang, S. H.; Di, Q. F.** (2000): Drilling extended reach well with rotary steering drilling system. *Acta Petrolei Sinica*, vol. 21, no. 1, pp. 76-80.
- Zhang, Q.; Jiang, B.; Huang, W. J.; Cui, W.; Liu, J. B.** (2018). Effect of wellhead tension on buckling load of tubular strings in vertical wells. *Journal of Petroleum Science and Engineering*, vol. 164, pp. 351-361.